



ISTITUTO NAZIONALE DI RICERCA METROLOGICA Repository Istituzionale

Stable and Reversible Lithium Storage Properties of LiTiOx Nanotubes for Electrochemical Recovery from Aqueous Solutions

Original

Stable and Reversible Lithium Storage Properties of LiTiOx Nanotubes for Electrochemical Recovery from Aqueous Solutions / Baudino, Luisa; Zaccagnini, Pietro; Garino, Nadia; Serrapede, Mara; Laurenti, Marco; Pedico, Alessandro; Pirri, C. Fabrizio; Lamberti, Andrea. - In: CHEMELECTROCHEM. - ISSN 2196-0216. - 9:10(2022). [10.1002/celc.202101652]

Availability:

This version is available at: 11696/77479 since:

Publisher:

Wiley

Published

DOI:10.1002/celc.202101652

Terms of use:

This article is made available under terms and conditions as specified in the corresponding bibliographic description in the repository

Publisher copyright

(Article begins on next page)

Stable and Reversible Lithium Storage Properties of LiTiO_x Nanotubes for Electrochemical Recovery from Aqueous Solutions

Luisa Baudino,^[a, b] Pietro Zaccagnini,^[a, b] Nadia Garino,^[a, b] Mara Serrapede,^[a, b]
Marco Laurenti,^[a, b] Alessandro Pedico,^[a] C. Fabrizio Pirri,^[a, b] and Andrea Lamberti^{*[a, b]}

In the present work, an easy and scalable method to prepare lithium titanium oxide nanotubes with stable and reversible lithium storage properties is reported. This material could be an excellent candidate for lithium recovery from aqueous solutions or have a direct application as Li-ion batteries electrodes in a circular economy perspective. Vertically oriented anatase nanotubes are grown by anodic oxidation in an ethylene glycol-based electrolyte. Then, the nanotubes are hydrothermally converted into a mixed lithium titanate. Morphological and

crystallographic characterizations confirm the successful shape-preserving conversion after which the nanotubes are subjected to electrochemical cycling. XRD and XPS analyses confirm a significant lithium uptake after cycling, and its recovery is investigated by means of an acidic treatment. While allowing for an almost complete recovery of the lithium integrated in their structure, the nanotubes also showed excellent morphological and structural stability proving to be excellent candidates for lithium recovery purposes.

Introduction

Nowadays, lithium is ever-present in the energy industry. Because of its capillary use in batteries for small electronics, electric vehicles and smart grids, one in three batteries commercially available is a lithium ion battery (LIB).^[1–4] Furthermore, batteries have become the first commercial use of lithium with their market share increasing from 30 % to around 60 % in the past years.^[5,6] The global market size of LIBs was recently estimated to grow up to USD 116.6 billion by 2030 from an already considerable USD 41.1 billion in 2021.^[7] Although applications are ever increasing, the same cannot be said of the availability of the element itself. Lithium can be found in ores and in water resources such as brines and seawater, which represent almost two thirds of its abundance on earth.^[5,8] Ores have been widely exploited for decades and are now degrading, and while evaporitic technologies are up-to-date and efficient they are also time and water-consuming.^[9] This led to an increasing interest in finding other ways to


harvest lithium from water resources like brines and in recycling spent batteries. In the frame of recovering lithium from solutions two different processes have been generally studied: physico-chemical adsorption and electrochemical techniques. The present study is focused on the recovery of lithium through the latter by means of pre-lithiated TiO_2 nanotubes grown by anodic oxidation on a titanium substrate.


The versatility of ordered 1D nanostructures has been widely investigated in the last decades. The first reports of TiO_2 nanotubes (NT) grown by anodic oxidation date to the early 2000s and since then the interest on this kind of self-organized structures has only grown.^[10,11] Applications of this kind of structure range from catalytic applications to photovoltaics to secondary batteries by exploiting its many interesting features.^[12–25] In particular, TiO_2 NTs grown by anodic oxidation on a conductive titanium foil have been extensively studied as electrodes for lithium ion batteries.^[26–35] In this case, the metal substrate work as current collector and the highly ordered structure of the NTs ensures a one-dimensional electronic and ionic conductivity.^[36] Pre-lithiation is a well-known strategy in the battery world to improve the electrochemical energy storage as is the use of spinels.^[37–41] Similarly, lithiated titanium oxide structures have recently been investigated to recover lithium from aqueous solutions as an alternative to lithium manganese oxide adsorbents due to their better stability in acidic solutions.^[42–46]

To the best of the authors' knowledge, this is the first systematic study on the stable and reversible lithium storage properties from ordered hydrothermally lithiated nanotubes obtained by anodic oxidation. Titania NTs were extensively studied as primarily anode materials for lithium ion batteries and thus galvanostatically tested, but only few works are available on the use of titania NTs as lithium adsorbents. Furthermore, these only focused on batch adsorption using the

[a] L. Baudino, Dr. P. Zaccagnini, Dr. N. Garino, Dr. M. Serrapede, Dr. M. Laurenti, Dr. A. Pedico, Prof. Dr. C. F. Pirri, Prof. Dr. A. Lamberti
Dipartimento di Scienza Applicata e Tecnologia (DISAT)
Politecnico di Torino
Corso Duca degli Abruzzi 24, 10129, Torino, Italy
E-mail: andrea.lamberti@polito.it

[b] L. Baudino, Dr. P. Zaccagnini, Dr. N. Garino, Dr. M. Serrapede, Dr. M. Laurenti, Prof. Dr. C. F. Pirri, Prof. Dr. A. Lamberti
Center for Sustainable Future Technologies
Istituto Italiano di Tecnologia
via Livorno 60, 10144, Torino, Italy

 Supporting information for this article is available on the WWW under <https://doi.org/10.1002/celec.202101652>

 © 2022 The Authors. ChemElectroChem published by Wiley-VCH GmbH. This is an open access article under the terms of the Creative Commons Attribution License, which permits use, distribution and reproduction in any medium, provided the original work is properly cited.

NTs as ion sieves.^[47,48] While Moazeni et al. used disordered NTs grown by hydrothermal processes, Taghvaei et al. calcinated the hydrothermally lithiated NTs grown by anodic oxidation. While the authors proved the adsorption properties through analyzing the composition of the solution pre and post adsorption, an accurate investigation of the properties of the adsorbent is still missing.

In the following, we propose a detailed study on the optimization of the lithiation conditions of TiO₂ anatase NT. Furthermore, we demonstrate that this kind of structure presents stable lithium storage properties while working in a reversible electrochemical setup and that its storing ability does not compromise the coulombic efficiency of the cell. Interestingly, we also demonstrate that lithium could be recovered after an acidic treatment that didn't compromise the structural stability nor the electrochemical behavior of the material. The use of acid leaching is a very popular strategy to recover lithium from spent batteries via hydrometallurgical processes. In this case the acid concentrations are usually quite high, up to 6 M, and the morphology of the specimens, which are previously crushed, is not conserved.^[49–52] On the other hand, when working with ion sieves in batch adsorption experiments, the adsorbents can be deposited in diluted acid baths to release the previously stored lithium.^[45,53–55] This elution treatment is generally considered to be the limiting step for the use of this kind of structures for lithium adsorption from aqueous resources. This is motivated by the fact that mixed oxides can undergo crystallographic changes and lose their structural integrity when exposed to acidic environments, thus making their prolonged application problematic. In this work we combine the two approaches by exposing the lithiated nanotubes to a solution of diluted HCl to leach the lithium stored during the electrochemical characterizations while maintaining its morphology and properties for further use. The peculiarity of the material herein proposed lies in its structural stability that allows its use for successive processes.

Results and Discussion

Optimization of synthesis parameters: effect of phase, temperature and LiOH concentration

As grown anatase nanotubes were characterized by FESEM and XRD to obtain information on the pristine samples and were afterwards used as reference samples. Different parameters were taken into consideration in order to optimize the hydrothermal conversion conditions, following a similar pattern of the one already employed by the group while investigating the structure of BaTiO₃.^[56,57] The influence of temperature, LiOH concentration and the phase of the pristine nanotubes were therefore investigated. XRD patterns of all the samples analyzed are shown in Figure 1. The insurgence of a mixed lithium/titanium oxide phase (LiTiO_x, indexed with circles) can be easily spotted by the appearance of the peak at 43.3° and the consequent reduction or disappearance of the strong peak at 25° typical of anatase phase (indexed with stars). The lithiation

of the anatase phase presents a very good repeatability as all the peaks of the LiTiO_x phase have been indexed with a cubic phase with an average Li:Ti ratio of 1:2. It is worth mentioning that at low temperatures (120°C and 150°C in Figure 1(a) and (b)) the conversion appears to be incomplete at low concentrations, with peaks of both the mixed oxide and the anatase phase present. Peaks indexed as lithium carbonate (triangles) can also be recognized in most of the high concentration samples at these temperatures as reaction by-products. Instead, at 200°C (Figure 1(c)) the conversion appears to be complete at all concentrations tested. A focus on the influence of the temperature and of the phase of the starting nanotubes can be seen in Figure 1(d). When comparing the four samples treated in LiOH 0.25 M, it can be seen that the only patterns reporting a successful conversion are the ones of amorphous and anatase nanotubes treated at 200°C. Under these conditions similar peaks of the same mixed oxide are obtained, although in the case of the amorphous sample the peak at 43° is broader and more asymmetrical hinting at a less ordered phase. FESEM images can easily confirm whether the conversion into the titanate morphology was successful or not. Pristine anatase nanotubes grown by anodic oxidation at 60 V for 15 minutes and annealed at 450°C for 30 minutes present a length between 6 and 7 μm (see Figure 2(a)) and a diameter of about 80–100 nm. The tubular morphology of the NTs was left unmodified when the conversion was unsuccessful, (see Figure S1 of the Supporting information) as the NTs remained in the anatase form. However, the morphology changed in the case of successful conversion, as was the case of the treatment for 2 hours at 200°C in LiOH 0.25 M (see Figure 2(b)). In this instance, the smooth surface was replaced by a very rough and particle-like structure protruding from the tubes.

By combining the results obtained on the morphology and crystallography of the samples analyzed the best hydrothermal conversion conditions were deemed to be the treatment in LiOH 0.25 M at 200°C for 2 hours on anatase nanotubes. The use of amorphous nanotubes was discarded since amorphous nanotubes are more unstable and tend to crystallize in anatase form when in contact with water solutions and provided the same mixed oxide after hydrothermal conversion.^[58]

Electrochemical characterizations

The suitability of the specimens as working electrodes in electrolytes containing lithium was investigated with electrochemical characterizations focused on the Li-insertion potential window. The cyclic voltammograms of the three different electrodes tested in LiPF₆ 1 M in EC:DMC 1:1 at 0.2 mV s^{−1} are reported in Figure 3. The TiO₂ anatase electrodes are represented with red squares, the LiTiO_x with blue circles and the lithiated phase subjected to acidic treatment (deLi-TiO_x) with black squares. Whereas the position of the lithiation peak appears to be quite similar (*V*_{red} between 1.66 V and 1.70 V), its shape changes considerably between the three cases. The anatase presents a very sharp peak because of the highly ordered structure, the lithiated and the partially de-lithiated

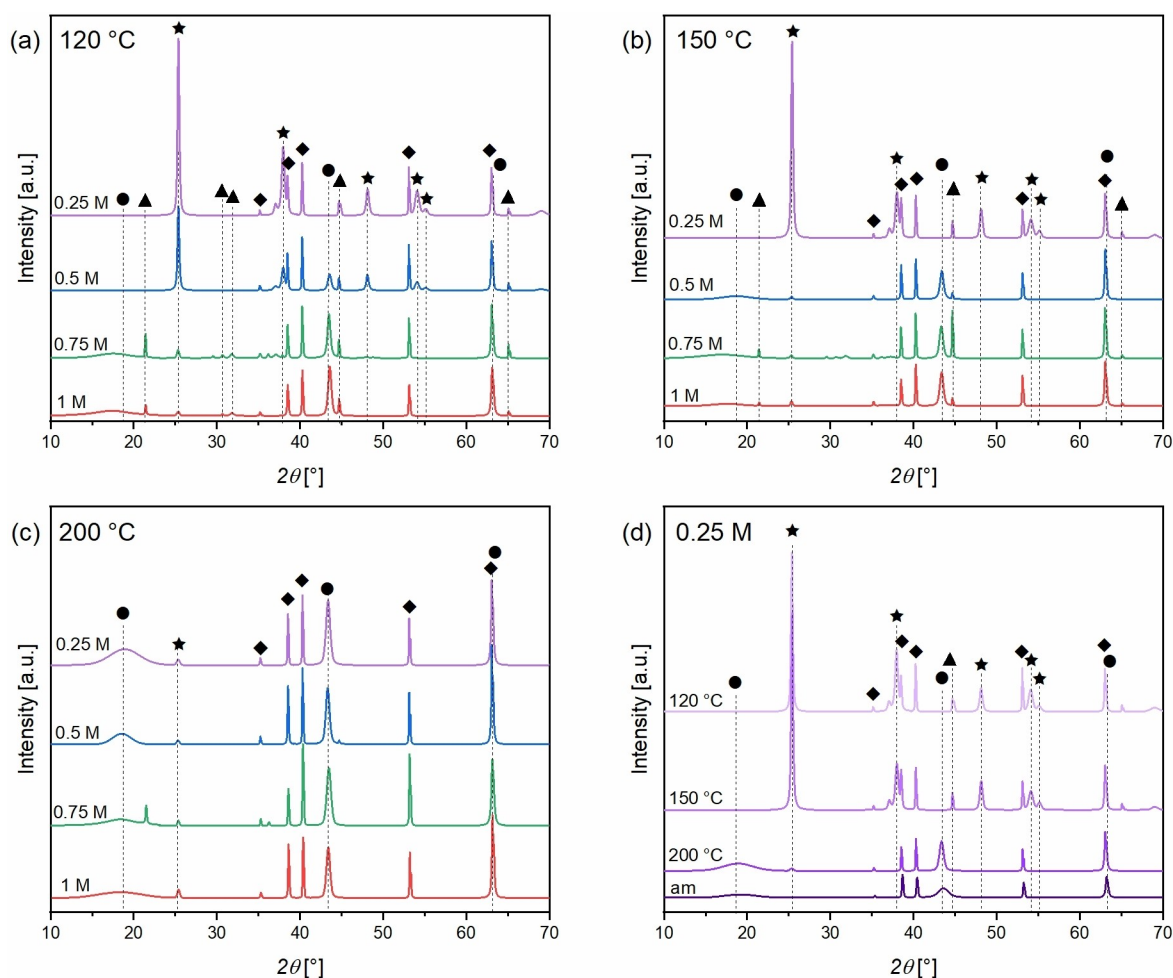


Figure 1. XRD diffractograms of the samples of TiO_2 nanotubes after the hydrothermal conversion. (a), (b), (c) Influence of temperature and concentration. Samples obtained after spending 2 hours in LiOH 0.25 M, 0.5 M, 0.75 M, 1 M at (a) 120 °C, (b) 150 °C, (c) 200 °C. (d) Effect of the temperature and phase: anatase NTs treated at 120 °C, 150 °C, 200 °C and amorphous NTs converted in LiOH 0.25 M at 200 °C. Stars (★) represent peaks of TiO_2 anatase, circles (●) the mixed oxide LiTiO_x , diamonds (◆) the titanium foil and triangles (▲) Li_2CO_3 .

phases have a broader one which is ascribable to a less ordered phase, as was evidenced by the micrograph, similar to what happens in amorphous electrodes. The de-lithiation peak position V_{ox} appears to vary with the phase considered, moving from 1.71 V to 2.14 V. The LiTiO_x appears to be the most reversible electrode of the three considered, as the distance between the two peaks is the smaller and about 0.5–0.6 V. Furthermore, it presents the maximum coulombic efficiency at such small scan rates. It is also possible to see that the anatase sample presents a second couple of peaks at about 1.41 V/1.74 V which has been known to be ascribable to the second phase transition from Li-poor Li_xTiO_2 to the titanate phase as reported in previous studies.^[36,59,60] The de-lithiated phase also presents a second peak in the lithiation portion of the voltammogram at around 2.17 V. Additional information such as specific capacity data are reported in Table 1.

The kinetic behavior of the electrodes was further investigated by performing cyclic voltammograms at increasing scan rates (up to 200 mVs^{-1}). By plotting the absolute value of the current density peaks versus the scan rates (see Figure S2 in the

Table 1. Electrochemical properties of the initial TiO_2 electrodes, the lithiated and de-lithiated samples at 0.2 mVs^{-1} .

	TiO_2 anatase	LiTiO_x	deLi- TiO_x
η_1	0.66	0.78	0.70
η_{max}	0.95	0.96	0.90
V_{red} [V]	1.70	1.65	1.67
Q_{ch} [mAh/cm ²]	0.175	0.120	0.190
V_{ox} [V]	2.14	1.71	1.84
Q_{dis} [mAh/cm ²]	0.115	0.124	0.134
EFB [V]	2.67	2.24	2.20
n [cm ⁻³]	5.56×10^{19}	3.78×10^{18}	4.69×10^{19}

Supporting information), it was possible to observe a linear dependence with the square root of the scan rate. This proved that the process was mainly diffusion-controlled in all the considered cases, contrary to other works that reported a predominance of pseudo capacitive behavior of anodically grown anatase nanotubes or hydrogen titanate and $\text{TiO}_2(\text{B})$ unidimensional nanostructures.^[61–64] Furthermore, the coulombic efficiency η of both the lithiated and de-lithiated samples reached values higher than 0.97 in every cycle at scan rates

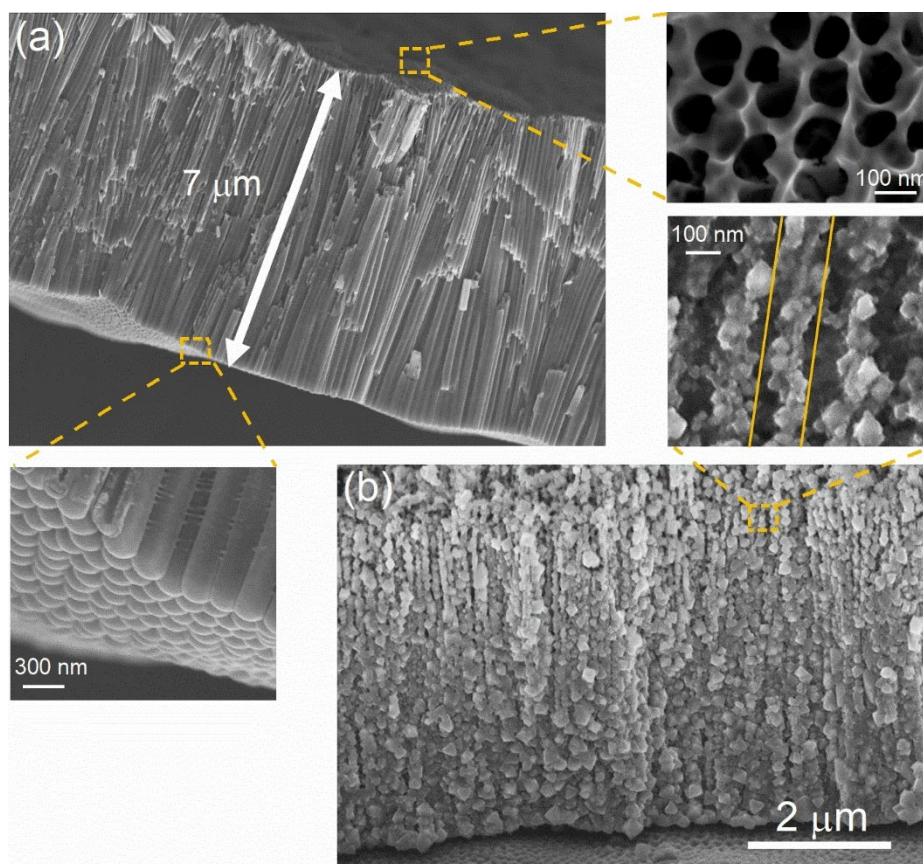


Figure 2. Morphological characterization of (a) pristine anatase nanotubes with insets of the top and bottom view, (b) nanotubes successfully converted into lithium titanate with an inset of the tubular morphology.

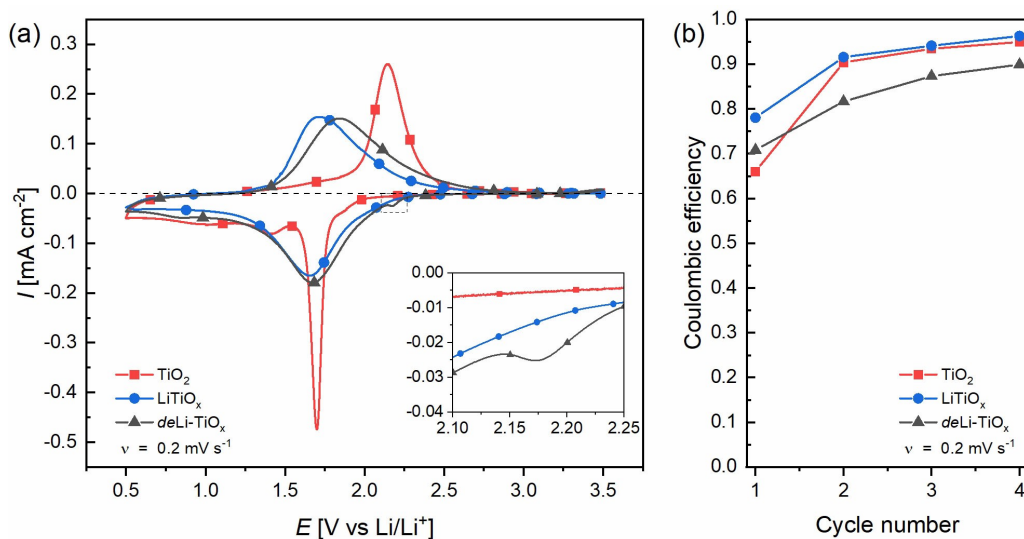


Figure 3. (a) Cyclic voltammograms and coulombic efficiencies of anatase (red squares), LiTiO_x (blue circles) and deLi-TiO_x (black triangles) at 0.2 mV s⁻¹ in LiPF₆ 1 M in EC:DMC 1:1.

higher than 0.5 mV s⁻¹, demonstrating the ability of this morphology to accommodate the structural changes due to further lithium intercalation/de-intercalation.

Mott Schottky measurements were performed on the three sets of electrodes to determine the carrier density N_D (referred to the geometrical area) and the flat band E_{FB} of the materials under study, following (eq. 1):

$$\frac{1}{C_s^2} = \frac{2}{\varepsilon_0 \varepsilon_r e N_D} \left(E - E_{FB} - \frac{kT}{e} \right) \quad (1)$$

with C_{SC} the differential capacitance of the space charge region, ε_0 the vacuum permittivity, E the applied potential, k , T and e have their conventional meaning. As a first approximation, the dielectric permittivity was considered to be 50 for TiO_2 anatase and the converted nanotubes.^[65] A more accurate value for the LiTiO_x is yet to be determined. Flat band potentials were respectively obtained from the intercept and slope of the linear fitting of the curves. The curves corresponding to 10 Hz can be found in Figure S3 of the Supporting information and the extrapolated properties are reported in Table 1. It is interesting to observe that the partially de-lithiated samples present similarities with both other electrodes. They show a similar flat band potential to the lithiated samples whereas the carrier density is closer to the one of anatase samples and about an order of magnitude higher than the one of the lithiated samples. The range of carriers obtained for all samples falls well into the one reported in literature.^[66]

Physico-chemical characterizations

XPS analyses were performed to further investigate the surface chemical properties of lithiated and de-lithiated NTs. Both samples were analyzed before and after the electrochemical characterization. The wide-energy XPS scans are reported in Figure S4 of the Supporting information and confirm the presence of lithium in all the analyzed samples. Further details were obtained by considering the HR spectral region for Li 1s (Figure 4). Each spectrum has been deconvoluted into separate components and the corresponding semi-quantitative results are summarized in Table S1 of the Supporting information. For the estimation of the amount of lithium effectively stored in the NT structure, only the component due to lithium/titanium phase has been considered. After the hydrothermal conversion, around 9 at.% of lithium could be stored in the NT structure. The Li 1s peak of the corresponding sample (Figure 4(a)) can be fitted with a single component positioned at 54.6 ± 0.1 eV and ascribed to the presence of a Li_2TiO_3 phase.^[67] The lithium storage capacity of the TiO_2 nanotubes was further improved after the electrochemical characterization; the amount of lithium inserted in the TiO_2 NT structure was almost doubled as it further increased up to around 17 at.%. The corresponding HR Li 1s spectrum (Figure 4(b)) has been deconvoluted into three

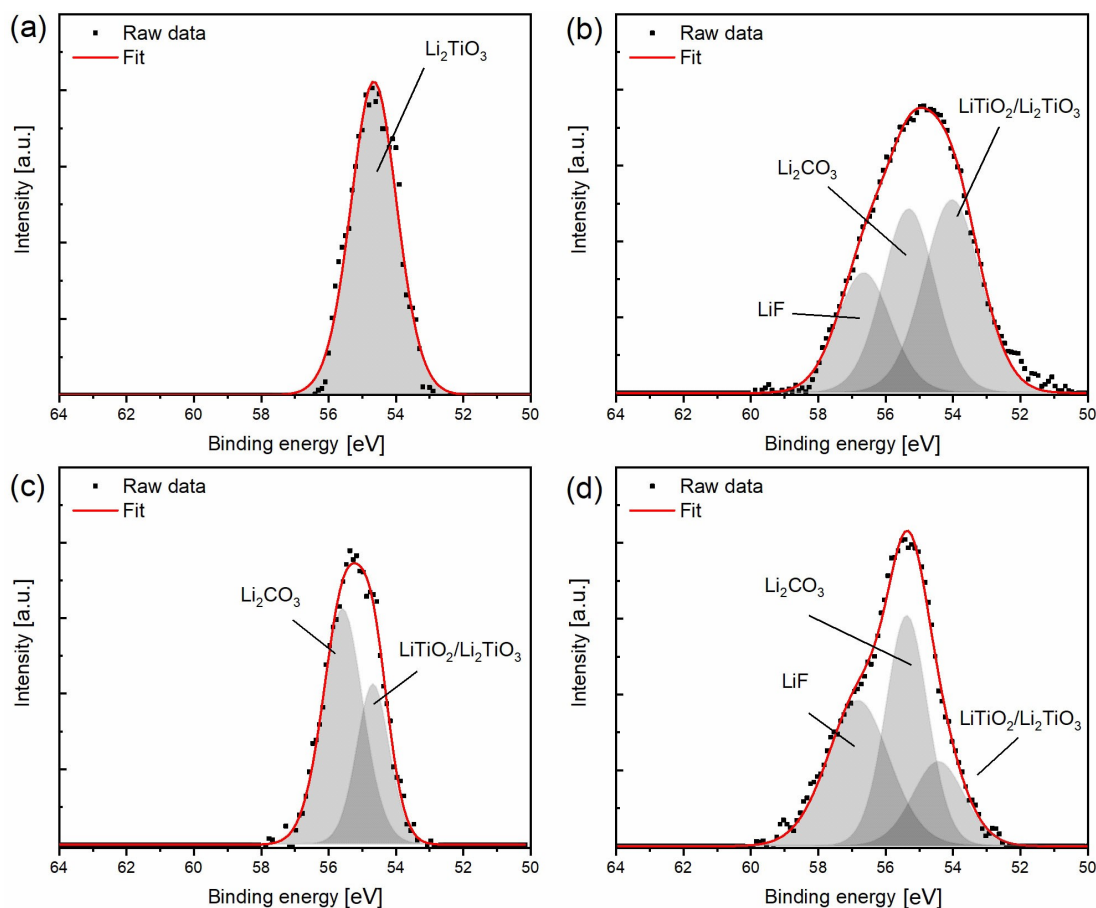


Figure 4. HR XPS acquisition of Li 1s region for (a) LiTiO_x NTs after the hydrothermal conversion, (b) LiTiO_x NTs after the electrochemical characterizations, (c) partially de-lithiated NTs and (d) partially de-lithiated NTs after the electrochemical characterizations.

separate components, positioned at 54.1 ± 0.1 eV, 55.4 ± 0.1 eV, and 56.7 ± 0.1 eV, and due to $\text{LiTiO}_2/\text{Li}_2\text{TiO}_3$ phase, lithium carbonates (Li_2CO_3) and LiF (coming from the electrolyte used during the electrochemical characterization),^[68] respectively. The co-existence of two separate lithium titanate species, i.e. LiTiO_2 and Li_2TiO_3 , is ascribed to the two different lithiation processes followed to insert lithium in the NT structure: the hydrothermal approach, leading to Li_2TiO_3 , and the electrochemical one, leading to LiTiO_2 . The above-mentioned distinction is visible by also considering the HR Ti 2p spectral region, shown in Figure S5 of the Supporting information. After hydrothermal conversion, the Ti 2p peak shows the presence of Ti^{4+} while both Ti^{4+} and Ti^{3+} valence states are observed after the electrochemical characterization, with the latter due to reduction of titania upon electrochemical lithium insertion.^[69] After de-lithiation in HCl, the amount of lithium previously stored in the NT structure decreased to around 4 at.%. In this case, deconvolution of the HR Li 1s peak (Figure 4(c)) in two components has been obtained, which are positioned at 54.7 ± 0.1 eV and 55.6 ± 0.1 eV, and due to $\text{LiTiO}_2/\text{Li}_2\text{TiO}_3$ phase and lithium carbonates (Li_2CO_3), respectively. A superior lithium storage could be found after cycling; the amount of Li re-stored in the TiO_2 NT structure (around 16 at.%) was around four times higher than the starting one (4 at.%). Similarly to the lithiated sample after the electrochemical characterization (Figure 4(b)), the HR Li 1s spectrum has been deconvoluted into three separate components due to $\text{LiTiO}_2/\text{Li}_2\text{TiO}_3$ phase, lithium carbonates (Li_2CO_3) and LiF (Figure 4(d)).

Even though de-lithiation has only been partially achieved, it is particularly interesting to notice that the structural integrity of the nanotubes was not compromised when extracting some of the lithium hydrothermally bonded. Zhang et al. reported that in the case of the de-lithiation of Li_2TiO_3 , the structure could be compromised when working at high concentrations and high temperatures.^[55] Bavykin et al. had also previously

commented on how titanate nanotubes could partially transform in rutile if exposed to acid environments for long periods of time, and Nakahira et al. also reported that acidic treatments led to structural disorders in the case of sodium titanates.^[70,71] Contrary to these previous works, the application here reported does not require temperatures higher than room temperature and was performed on shorter times. Moreover, it is worth noticing that in our case the nanotubes underwent no crystallographic changes during the de-lithiation (no rutile peaks are present in the XRD diffractograms reported in Figure 5(a)) and the material was able to fully recover to higher lithium contents when cycled, thus exhibiting an excellent reversible behavior. The morphology of all the samples of nanotubes was also conserved throughout the whole process, as evidenced by the micrograph reported in Figure 5(b). Systematic studies to further clarify the de-lithiation mechanisms of our material are still ongoing.

A systematic comparison between the diffractograms of the partially de-lithiated and lithiated phases can be seen in Figure 5(a). The peaks in the two cases are very similar, but in the de-lithiated case the intensity is lower and the peaks are slightly asymmetric and shifted to 0.5° higher. These small changes in the XRD signature of the de-lithiated phase are in agreement with what previously reported in the literature.^[48,72] Furthermore, the XRD diffractograms confirmed a change in the lithiated phase of the nanotubes after the cycling, as was seen with XPS analyses. This change is underlined by the disappearance of the peak at 18° , the shift from 43° to 44.5° of its most intense one and the split of the one at 63° into two smaller peaks. The new phase indexed in Figure 5(a) with reversed triangles, resulted to be richer in lithium and was indexed with a cubic mixed oxide in which the average Li:Ti ratio was shifted from 1:2 to 2:1. These results, although not providing a stoichiometric compound, are in good agreement with the data obtained by XPS in which two different kinds of titanates were

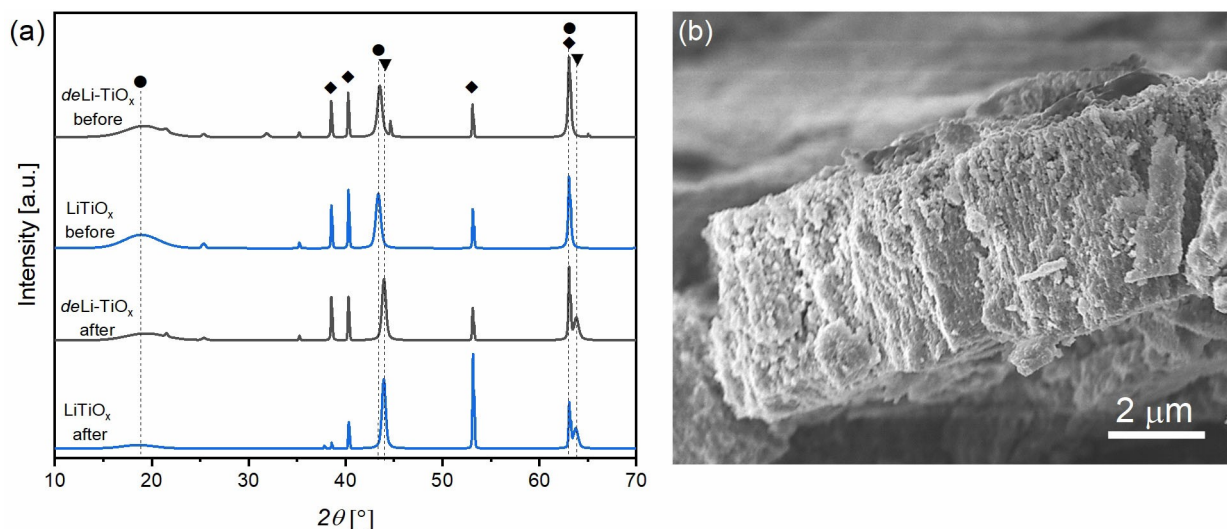


Figure 5. (a) XRD patterns of the lithiated and de-lithiated samples before and after the galvanostatic cycling. Circles (●) index the Li-poor mixed phase of LiTiO_x , diamonds (◆) the Titanium foil, reversed triangles (▼) the Li-rich phase of LiTiO_x ; (b) FESEM micrograph of the LiTiO_x nanotubes after galvanostatic cycling.

present in our samples as a result of the two different lithiation mechanisms.

Conclusion

This work provided a detailed study on the hydrothermal conversion of anodized titania nanotubes into a mixed LiTiO_x . After optimizing the hydrothermal conversion conditions, the suitability of the NTs as electrodes for lithium adsorption was demonstrated in an organic electrolyte under electrochemical conditions. This was an important first test of the material before envisaging its application to aqueous solutions. Morphological characterizations confirmed that the structure of the nanotubes was conserved after the electrochemical tests. Compositional analyses reported an impressive amount of lithium stored into the structure of the nanotubes, increasing from 9 at.% to 17 at.%. The reversibility of lithium storage properties of the electrode was deeply investigated by static de-lithiation, which highlighted that neither the structural stability of the nanotubes nor their electrochemical performances were compromised when almost all of the lithium was extracted from them. Furthermore, the de-lithiated structure reached the same quantity of lithium stored after the electrochemical characterizations as the pre-lithiated sample, proving the reversible behavior of our material as lithium adsorbent. Its excellent performance under acidic conditions proves its potential to recover lithium from unconventional resources, as this is known to be the most critical step of the harvesting process during which adsorbents may become unstable. Otherwise, these nanotubes could be directly used as electrodes in Li-ion batteries systems as they have proved to be excellent candidates for this kind of application.

Experimental Section

Synthesis: Anodic oxidation

Titanium dioxide nanotubes (NTs) were grown on Titanium foil (0.1 mm, > 99.9%, MTI Corporation) by anodic oxidation following a procedure previously reported.^[73,74] Samples were pre-treated by sonication in deionized water (DIW) for 10 min and etching in HF 1 wt.% (40%, Carlo Erba) followed by abundant rinsing in DIW. The two-step anodic oxidation was performed in a thermostatic bath at 25 °C under continuous stirring, in an EG-based electrolyte. The electrolyte contained 2.5 wt.% of DIW, 0.5 wt.% of ammonium fluoride (> 98%, Sigma Aldrich) in EG ($\geq 99.5\%$, Honeywell). Substrates of Ti foil were used as both working and counter electrodes. During the first step 60 V were applied for 5 minutes with a constant power generator (GW Instek SPD-3606), at the end of which the NTs layer was removed by ultrasonically cleaning the samples in hydrogen peroxide (Sigma Aldrich) to obtain the tube template on the substrate. A constant potential of 60 V was then applied for 15 minutes to grow a new layer of amorphous nanotubes after which the samples were thoroughly rinsed in deionized water. The samples were then annealed at 450 °C for 30 minutes to crystallize them in anatase phase.

Hydrothermal conversion

The hydrothermal conversion of the anatase NTs was performed in Teflon-lined stainless-steel acid-digestion vessels (Parr general purpose acid digestion vessel 23 mL, Parr Instrument Company, Moline, IL). To investigate the influence of the alkaline solution, samples were treated in lithium hydroxide solutions (LiOH monohydrate, > 99%, Alfa Aesar) with concentrations between 0.25 M and 1 M. The samples were immersed in the reactor, filled to 50% of its capacity, and heated for 2 hours in a muffle furnace (Muffle Furnace L9/11, Nabertherm GmbH). To determine the effect of the temperature, the treatment was performed at 120 °C, 150 °C and 200 °C. Once cooled and removed from the reactors, the lithiated samples were rinsed in DIW and dried under nitrogen flow before the characterizations.

Characterizations

Morphological characteristics of the samples were obtained through Field Emission Scanning Electron Microscopy (FESEM Supra 40, Zeiss, Oberkochen, Germany) equipped with a Si(Li) detector (Oxford Instruments, Abington, UK) for energy-dispersive X-ray spectroscopy. The samples crystallography was investigated with a Panalytical X'Pert MRD Pro X-ray diffractometer with a $\text{Cu K}\alpha$ source before and after the cycling, and the diffractograms obtained were analyzed with the HighScore Plus software. The surface composition was analyzed by X-Ray Photoelectron Spectroscopy (XPS) both before and after the electrochemical characterizations on all the different kind of electrodes. XPS measurements (analyzed area $500\text{ }\mu\text{m} \times 500\text{ }\mu\text{m}$) have been performed with a PHI 5000 VersaProbe system (from Physical Electronic), equipped with $\text{Al K}\alpha$ radiation (1486.6 eV) as X-ray source. Wide-energy and high-resolution (HR) XPS spectra were collected and processed using CasaXPS software (version 2.3.18). HR spectra deconvolution into individual mixed Gaussian-Lorentzian peaks was obtained after Shirley background subtraction and binding energy (BE) calibration according to C 1s position for adventitious carbon (284.8 eV). Semi-quantitative analyses were obtained from the analysis of HR XPS acquisitions.

Electrochemical characterizations were performed in three-electrode PAT-Cells (EL-CELL GmbH) connected to a VMP3 Potentiostat by BioLogic with EC-Lab V11.34 Software. The measurement setup comprises a lithium ring reference with double-layered FS-5P separator (200 μm , EL-CELL GmbH) and a highly capacitive carbon-based counter electrode. Counter electrodes consisted of 85 wt.% activated carbon (Kuraray Active Carbon), 10 wt.% carbon black (Timical Super C45) and 5 wt.% PTFE (60 wt.% dispersion in H_2O , Sigma Aldrich). Working and counter electrodes diameters was 18 mm thus 2.54 cm^2 geometric area. All measurements were done in organic lithium hexafluorophosphate based electrolyte (LiPF_6 1 M in EC:DMC 1:1 Solvionic E00350) after drying the samples overnight at 120 °C. Cyclic voltammetries were performed between 3.5 V vs Li/Li^+ and 0.5 V vs Li/Li^+ with scan rates in linear and square root spacing in three decades (0.2 mVs^{-1} to 200 mVs^{-1}), starting from open circuit potential. The current was measured over the second half of each step and averaged ten voltage steps. Four cycles were performed for scan rates under 2 mVs^{-1} , then six cycles for scan rates between 2 mVs^{-1} and 10 mVs^{-1} and finally 11 cycles for higher scan rates. Electrochemical impedance spectroscopy measurements were carried out in the 10^{-2} – 10^5 Hz frequency range with an AC signal of 5 mV. Mott Schottky impedance measurements were performed in the same potential window as the cyclic voltammetries with a potential step of 0.1 V. During potentiostatic measurements the instrument resolution was kept constant at 100 μV . Bandwidth was selected according to spectroscopic measurements to let the system being stable.

Some of the lithiated samples were subjected to an acidic bath of HCl 0.1 M (Hydrochloric acid 37%, Sigma Aldrich) for 48 hours at room temperature to investigate a possible de-lithiation of the mixed oxide and assess the recyclability of the adsorbent. This was performed in an Aqu EC Cell (EL-Cell GmbH) with 30 µl of acid solution and Silver 20 separator (DreamWeaver). The lithiated electrodes were in a symmetric configuration. Following this de-lithiation process the electrodes (called deLi-TiOx) underwent the electrochemical characterizations already described.

Acknowledgements

This paper has been possible thanks to the funding of the Italian Ministry of Economic Development's Directorate General for Safety – National Mining Office for Hydrocarbons and Georesources. Open Access Funding provided by Politecnico di Torino within the CRUI-CARE Agreement.

Conflict of Interest

The authors declare no conflict of interest.

Data Availability Statement

The data that support the findings of this study are available from the corresponding author upon reasonable request.

Keywords: Anodic oxidation • Lithium • Nanotubes • Raw material recovery • Titanates

- [1] C. Grosjean, P. Herrera Miranda, M. Perrin, P. Poggi, *Renewable Sustainable Energy Rev.* **2012**, *16*, 1735–1744.
- [2] T. P. Narins, *Extr. Ind. Soc.* **2017**, *4*, 321–328.
- [3] IEA, *Global EV Outlook 2019*, OECD, Paris, 2019.
- [4] F. Meng, J. McNeice, S. S. Zadeh, A. Ghahreman, *Miner. Process. Extr. Metall. Rev.* **2019**, *00*, 1–19.
- [5] B. Swain, *Sep. Purif. Technol.* **2017**, *172*, 388–403.
- [6] United States Geological Survey, *Mineral Commodity Summaries* **2020**, 2020.
- [7] MarketsandMarkets, *Lithium-Ion Battery Market with COVID-19 Impact Analysis, by Type (Li-NMC, LFP, LCO, LTO, LMO, NCA), Capacity, Voltage, Industry (Consumer Electronics, Automotive, Power, Industrial), & Region (North America, Europe, APAC & RoW) - Global Forecast to 2030*, 2021.
- [8] P. W. Gruber, P. A. Medina, G. A. Keoleian, S. E. Kesler, M. P. Everson, T. J. Wallington, *J. Ind. Ecol.* **2011**, *15*, 760–775.
- [9] V. Flexer, C. F. Baspineiro, C. I. Galli, *Sci. Total Environ.* **2018**, *639*, 1188–1204.
- [10] V. Zwilling, M. Aucouturier, E. Darque-Ceretti, *Electrochim. Acta* **1999**, *45*, 921–929.
- [11] D. Gong, C. A. Grimes, O. K. Varghese, W. Hu, R. S. Singh, Z. Chen, E. C. Dickey, *J. Mater. Res.* **2001**, *16*, 3331–3334.
- [12] Y. C. Nah, I. Paramasivam, P. Schmuki, *ChemPhysChem* **2010**, *11*, 2698–2713.
- [13] P. Roy, S. Berger, P. Schmuki, *Angew. Chem. Int. Ed.* **2011**, *50*, 2904–2939; *Angew. Chem.* **2011**, *123*, 2956–2995.
- [14] J.-Y. Y. Liao, J.-W. W. He, H. Xu, D.-B. Bin Kuang, C.-Y. Y. Su, *J. Mater. Chem.* **2012**, *22*, 7910.
- [15] H. P. Jen, M. H. Lin, L. L. Li, H. P. Wu, W. K. Huang, P. J. Cheng, E. W. G. Diau, *ACS Appl. Mater. Interfaces* **2013**, *5*, 10098–10104.
- [16] M. Ge, C. Cao, J. Huang, S. Li, Z. Chen, K. Q. Zhang, S. S. Al-Deyab, Y. Lai, *J. Mater. Chem. A* **2016**, *4*, 6772–6801.
- [17] M. Krbal, S. Ng, M. Motola, L. Hromadko, F. Dvorak, V. Prokop, H. Sopha, J. M. Macak, *Appl. Mater. Res.* **2019**, *17*, 104–111.
- [18] F. Dvorak, M. Zazpe, M. Krbal, H. Sopha, J. Prikyr, S. Ng, L. Hromadko, F. Bures, J. M. Macak, *Appl. Mater. Res.* **2019**, *14*, 1–20.
- [19] J. Bi, X. Huang, J. Wang, Q. Tao, T. Wang, H. Hao, *J. Mater. Chem. A* **2020**, *8*, 14415–14440.
- [20] A. Kupferer, A. Holm, A. Lotnyk, S. Mändl, S. G. Mayr, *Adv. Funct. Mater.* **2021**, *31*, 2104250.
- [21] L. Lin, Z. Lu, W. Zhang, *Resour. Conserv. Recycl.* **2021**, *167*, 105416.
- [22] S. Wang, H. Sun, P. Qiao, Z. Li, Y. Xie, W. Zhou, *Appl. Mater. Res.* **2021**, *22*, 100977.
- [23] A. Touni, X. Liu, X. Kang, P. A. Carvalho, S. Diplas, K. G. Both, S. Sotiropoulos, A. Chatzidakis, *ChemSusChem* **2021**, *14*, 4993–5003.
- [24] S. Mohajernia, S. Hejazi, P. Andryskova, G. Zoppellaro, O. Tomanec, R. Zboril, P. Schmuki, *ChemElectroChem* **2019**, *6*, 1244–1249.
- [25] L. Razzaboni, M. Altomare, M. Pedferri, M. V. Diamanti, P. Schmuki, *ChemElectroChem* **2020**, *7*, 2859–2863.
- [26] M. C. López, G. F. Ortiz, J. R. González, R. Alcántara, J. L. Tirado, *ACS Appl. Mater. Interfaces* **2014**, *6*, 5669–5678.
- [27] D. Pan, H. Huang, X. Wang, L. Wang, H. Liao, Z. Li, M. Wu, *J. Mater. Chem. A* **2014**, *2*, 11454–11464.
- [28] J. Brumbarov, J. P. Vivek, S. Leonardi, C. Valero-Vidal, E. Portenkirchner, J. Kunze-Liebhäuser, *J. Mater. Chem. A* **2015**, *3*, 16469–16477.
- [29] M. Madian, L. Giebler, M. Klose, T. Jaumann, M. Uhlemann, A. Gebert, S. Oswald, N. Ismail, A. Eychmüller, J. Eckert, *ACS Sustainable Chem. Eng.* **2015**, *3*, 909–919.
- [30] W. Wen, J. M. Wu, Y. Z. Jiang, J. Q. Bai, L. L. Lai, *J. Mater. Chem. A* **2016**, *4*, 10593–10600.
- [31] M. Zhang, K. Yin, Z. D. Hood, Z. Bi, C. A. Bridges, S. Dai, Y. S. Meng, M. P. Paranthaman, M. Chi, *J. Mater. Chem. A* **2017**, *5*, 20651–20657.
- [32] G. D. Salián, M. Krbal, H. Sopha, C. Lebouin, M.-V. Coulet, J. Michalicka, L. Hromadko, A. T. Tesfaye, J. M. Macak, T. Djenizian, *Appl. Mater. Res.* **2019**, *16*, 257–264.
- [33] T. Tian, L.-L. Lu, Y.-C. Yin, F. Li, T.-W. Zhang, Y.-H. Song, Y.-H. Tan, H.-B. Yao, *Adv. Funct. Mater.* **2021**, *31*, 2007419.
- [34] Y. Lu, J. Wang, Y. Chen, X. Zheng, H. Yao, S. Mathur, Z. Hong, *Adv. Funct. Mater.* **2021**, *31*, 2009605.
- [35] N. A. Kyeremateng, *ChemElectroChem* **2014**, *1*, 1442–1466.
- [36] A. Auer, E. Portenkirchner, T. Götsch, C. Valero-Vidal, S. Penner, J. Kunze-Liebhäuser, *ACS Appl. Mater. Interfaces* **2017**, *9*, 36828–36836.
- [37] J. Haetge, P. Hartmann, K. Brezesinski, J. Janek, T. Brezesinski, *Chem. Mater.* **2011**, *23*, 4384–4393.
- [38] G. Ji, Y. Ma, B. Ding, J. Y. Lee, *Chem. Mater.* **2012**, *24*, 3329–3334.
- [39] K. Zou, W. Deng, P. Cai, X. Deng, B. Wang, C. Liu, J. Li, H. Hou, G. Zou, X. Ji, *Adv. Funct. Mater.* **2020**, *2005581*, 1–23.
- [40] F. Wang, B. Wang, J. Li, B. Wang, Y. Zhou, D. Wang, H. Liu, S. Dou, *ACS Nano* **2021**, *acs.nano.0c10664*.
- [41] L. Jin, C. Shen, Q. Wu, A. Shellikeri, J. Zheng, C. Zhang, J. P. Zheng, *Adv. Sci.* **2021**, *8*, 2005031.
- [42] M. M. Thackeray, *J. Am. Ceram. Soc.* **2004**, *82*, 3347–3354.
- [43] Z. Hong, M. Wei, *J. Mater. Chem. A* **2013**, *1*, 4403–4414.
- [44] T.-F. Yi, S.-Y. Yang, Y. Xie, *J. Mater. Chem. A* **2015**, *3*, 5750–5777.
- [45] L. A. Limjoco, G. M. Nisola, C. P. Lawagon, S. P. Lee, J. G. Seo, H. Kim, W.-J. Chung, *Colloids Surf. A* **2016**, *504*, 267–279.
- [46] S. Safari, B. G. Lottermoser, D. S. Alessi, *Appl. Mater. Res.* **2020**, *19*, 100638.
- [47] M. Moazeni, H. Hajipour, M. Askari, M. Nusheh, *Mater. Res. Bull.* **2015**, *61*, 70–75.
- [48] N. Taghvaei, E. Taghvaei, M. Askari, *ChemistrySelect* **2020**, *5*, 10339–10345.
- [49] Y. Guo, F. Li, H. Zhu, G. Li, J. Huang, W. He, *Waste Manage.* **2016**, *51*, 227–233.
- [50] A. Porvali, M. Aaltonen, S. Ojanen, O. Velazquez-Martinez, E. Eronen, F. Liu, B. P. Wilson, R. Serna-Guerrero, M. Lundström, *Resour. Conserv. Recycl.* **2019**, *142*, 257–266.
- [51] F. Arshad, L. Li, K. Amin, E. Fan, N. Manurkar, A. Ahmad, J. Yang, F. Wu, R. Chen, *ACS Sustainable Chem. Eng.* **2020**, *8*, 13527–13554.
- [52] K. Du, E. H. Ang, X. Wu, Y. Liu, *Energy Environ. Mater.* **2022**, DOI 10.1002/eem2.12271.
- [53] L. Zhang, D. Zhou, G. He, F. Wang, J. Zhou, *Mater. Lett.* **2014**, *135*, 206–209.
- [54] C. P. Lawagon, G. M. Nisola, J. Mun, A. Tron, R. E. C. Torrejos, J. G. Seo, H. Kim, W.-J. Chung, *J. Ind. Eng. Chem.* **2016**, *35*, 347–356.

- [55] L. Zhang, G. He, D. Zhou, J. Zhou, Q. Yao, *Ionics* **2016**, *22*, 2007–2014.
- [56] A. Lamberti, N. Garino, K. Bejtka, S. Bianco, S. Stassi, A. Chiodoni, G. Canavese, C. F. Pirri, M. Quaglio, *New J. Chem.* **2014**, *38*, 2024–2030.
- [57] J. A. Muñoz-Tabares, K. Bejtka, A. Lamberti, N. Garino, S. Bianco, M. Quaglio, C. F. Pirri, A. Chiodoni, *Nanoscale* **2016**, *8*, 6866–6876.
- [58] A. Lamberti, A. Chiodoni, N. Shahzad, S. Bianco, M. Quaglio, C. F. Pirri, *Sci. Rep.* **2015**, *5*, 7808.
- [59] M. Wagemaker, W. J. H. H. Borghols, F. M. Mulder, *J. Am. Chem. Soc.* **2007**, *129*, 4323–4327.
- [60] W. J. H. Borghols, D. Lützenkirchen-Hecht, U. Haake, E. R. H. van Eck, F. M. Mulder, M. Wagemaker, *Phys. Chem. Chem. Phys.* **2009**, *11*, 5742–5748.
- [61] J. Li, Z. Tang, Z. Zhang, *Chem. Mater.* **2005**, *17*, 5848–5855.
- [62] M. Zúkalová, M. Kalbáč, L. Kavan, I. Exnar, M. Graetzel, *Chem. Mater.* **2005**, *17*, 1248–1255.
- [63] K. Zhu, Q. Wang, J. Kim, A. A. Pesaran, A. J. Frank, *J. Phys. Chem. C* **2012**, *116*, 11895–11899.
- [64] L. Kavan, M. Kalbáč, M. Zúkalová, I. Exnar, V. Lorenzen, R. Nesper, M. Graetzel, *Chem. Mater.* **2004**, *16*, 477–485.
- [65] R. van de Krol, A. Goossens, J. Schoonman, *J. Phys. Chem. B* **1999**, 7151–7159.
- [66] A. G. Muñoz, *Electrochim. Acta* **2007**, *52*, 4167–4176.
- [67] S. Gu, B. Ji, Q. Qi, J. Wang, H. Zhou, Y. Zhang, G. Luo, *Int. J. Hydrogen Energy* **2019**, *44*, 32151–32157.
- [68] I. Ismail, A. Noda, A. Nishimoto, M. Watanabe, *Electrochim. Acta* **2001**, *46*, 1595–1603.
- [69] D. Steiner, A. Auer, E. Portenkirchner, J. Kunze-Liebhäuser, *J. Electroanal. Chem.* **2018**, *812*, 166–173.
- [70] D. V. Bavykin, J. M. Friedrich, A. A. Lapkin, F. C. Walsh, *Chem. Mater.* **2006**, *18*, 1124–1129.
- [71] A. Nakahira, T. Kubo, C. Numako, *ACS Appl. Mater. Interfaces* **2010**, *2*, 2611–2616.
- [72] R. Chitrakar, Y. Makita, K. Ooi, A. Sonoda, *Dalton Trans.* **2014**, *43*, 8933–8939.
- [73] A. Lamberti, N. Garino, A. Sacco, S. Bianco, A. Chiodoni, C. Gerbaldi, *Electrochim. Acta* **2015**, *151*, 222–229.
- [74] A. Lamberti, D. Manfredi, F. Calignano, C. F. Pirri, *Mater. Today Commun.* **2018**, *15*, 165–170.

Manuscript received: December 14, 2021

Revised manuscript received: February 14, 2022

Accepted manuscript online: February 15, 2022

Recovery from Aqueous Solutions

